Journal of
Composites Science

MDPI

Article

Effective CdS:(Ce, Ga) Nanoparticles for Photocatalytic H_2 Production Under Artificial Solar Light Exposer

Pedda Thimmula Poojitha [1], Radhalayam Dhanalakshmi [2], Mohammad Rezaul Karim [3], Sung Jin An [4], Kummara Madhusudana Rao [5,*], Siva Pratap Reddy Mallem [6,*] and Young Lae Kim [1,*]

[1] Department of Electronic Engineering, Gangneung-Wonju National Univeristy, Gangneung 25457, Republic of Korea; ptpoojitha.email@gmail.com
[2] Department of Physics, University of Santiago of Chile (USACH), Santiago 9170124, Chile; dhanalakshmi.radhalayam@usach.cl
[3] Center of Excellence for Research in Engineering Materials (CEREM), Deanship of Scientific Research, King Saud University, Riyadh 11421, Saudi Arabia; karim@ksu.edu.sa
[4] Department of Materials Science and Engineering, Kumoh National Institute of Technology, Gumi 39177, Republic of Korea; sungjinan@kumoh.ac.kr
[5] School of Chemical Engineering, Yeungnam University, 280 Daehak-Ro, Gyeongsan 38541, Republic of Korea
[6] Advanced Material Research Center, Kumoh National Institute of Technology, Gumi 39177, Republic of Korea
* Correspondence: msraochem@gmail.com (K.M.R.); drmspreddy@kumoh.ac.kr (S.P.R.M.); ylkim@gwnu.ac.kr (Y.L.K.)

Abstract: To encounter the burgeoning energy demands of the future, it is imperative to focus on the progress of innovative and profitable techniques for hydrogen (H_2) evolution, coupled with an enriched stability of photocatalysts. In this work, we have effectually prepared CdS, CdS:Ce, and CdS:(Ce, Ga) nanoparticles through a chemical refluxing method at 120 °C. Comprehensive structural analysis confirmed the effectual incorporation of Ce and Ga ions in the place of Cd^{2+} in a CdS matrix. Morphology analysis indicates that the prepared samples are irregularly shaped nanoparticles. Chemical analysis confirmed that the Ce and Ga ions incorporated in the Cd site occurred with 3+ and 4+ valence states. All the samples were assessed for H_2 production through water splitting via artificial solar light irradiation. Amid all the samples, CdS:(Ce, Ga) nanoparticles portrayed a giant H_2 evolution efficacy (3012 μmol $h^{-1}g^{-1}$) in 300 min, which is 13.9 times larger than that of the bar CdS sample. Thus, we firmly propose that CdS:(Ce, Ga) samples are authentic and potent candidates for efficient photocatalytic H_2 production in sterile environments.

Keywords: cadmium sulfide; hydrogen evolution; co-doping

check for updates

Academic Editor: Francesco Tornabene

Received: 26 November 2024
Revised: 22 December 2024
Accepted: 8 January 2025
Published: 13 January 2025

Citation: Poojitha, P.T.; Dhanalakshmi, R.; Karim, M.R.; An, S.J.; Madhusudana Rao, K.; Mallem, S.P.R.; Kim, Y.L. Effective CdS:(Ce, Ga) Nanoparticles for Photocatalytic H_2 Production Under Artificial Solar Light Exposer. *J. Compos. Sci.* **2025**, *9*, 34. https://doi.org/10.3390/jcs9010034

Copyright: © 2025 by the authors. Licensee MDPI, Basel, Switzerland. This article is an open access article distributed under the terms and conditions of the Creative Commons Attribution (CC BY) license (https://creativecommons.org/licenses/by/4.0/).

1. Introduction

In recent decades, the accelerating rise in Earth's average temperature—driven by rapid urbanization, industrial expansion, and unprecedented population growth—has escalated concerns about global warming and climate change. Among the numerous contributors to this crisis, environmental contamination from the intensive use of fossil fuels is particularly alarming. Addressing these challenges requires a transition to renewable and sustainable energy sources to curb greenhouse gas emissions and promote long-term environmental resilience. Hydrogen production, especially through photocatalytic processes, is emerging as a pivotal element in this global energy transition due to its potential as a clean and efficient fuel.

Solar energy, harnessed for hydrogen (H_2) production via photocatalytic water splitting, is gaining traction as a sustainable alternative to traditional energy systems [1,2].

Conducting this process at the nanoscale, particularly on semiconductor surfaces, significantly enhances efficiency. The increased surface-to-volume ratio and quantum confinement effects at the nanoscale improve light absorption, charge separation, and reaction kinetics compared to bulk materials. Furthermore, semiconductor nanostructures host a substantial density of charge carriers on their surfaces, directly influencing their physicochemical properties and catalytic activity [3,4].

Among various semiconductor materials, systems based on II-VI compounds, such as cadmium sulfide (CdS), have gained prominence due to their ability to efficiently absorb visible light, generate high charge-carrier densities, and effectively separate photogenerated electron–hole pairs. These properties make them highly suitable for hydrogen evolution through water splitting [5–7]. CdS-based photocatalysts have shown promising results in experimental setups, with their versatility extending across multiple industrial and environmental applications [8–11].

Despite these advantages, the photocatalytic performance of pure CdS in aqueous environments is hindered by issues such as structural decomposition, photogenerated charge recombination, and susceptibility to photo-corrosion during hydrogen evolution. To overcome these challenges, various strategies—such as the fabrication of composites, surface decoration with co-catalysts, and the introduction of mono- or co-doping—have been employed to enhance their stability and catalytic efficiency. Notably, doping techniques introduce additional charge carriers and defect sites, effectively reducing charge recombination and enabling efficient hydrogen production [12,13].

In this study, we report the fabrication of CdS nanoparticles, as well as their Ce-doped (CdS:Ce) and (Ce, Ga) co-doped (CdS:(Ce, Ga)) counterparts, and explore their photocatalytic performance for hydrogen production. Our investigation offers the first comprehensive insights into the impact of Ce-doping and (Ce, Ga) co-doping on the photocatalytic H_2 evolution properties of CdS nanoparticles. These modifications not only enhance their photocatalytic activity but also provide a pathway for their potential integration into industrial hydrogen production systems, which are pivotal for advancing the global shift toward a hydrogen-based energy economy.

2. Materials and Methods

2.1. Materials

All specimens were synthesized by employing a straightforward chemical refluxing technique. The precursor compounds, namely cadmium acetate dihydrate [$Cd(CH_3COO)_2{\cdot}2H_2O$], sodium sulfide nonahydrate [$Na_2S{\cdot}9H_2O$], gallium nitrate hydrate [$Ga(NO_3)_3 \cdot xH_2O$], and cerium chloride heptahydrate [$CeCl_3{\cdot}7H_2O$], were procured from Merk. Initially, solutions containing 0.01 M of cadmium acetate paired with gallium nitrate and cerium chloride in varying combinations—(0.133 g + 0 + 0) for bare CdS, (0.127 g + 0.007 g + 0) for CdS:Ce, and (0.122 g + 0.007 g + 0.005 g) for CdS:(Ce, Ga)—were dissolved in 50 mL of deionized water and vigorously stirred at 120 °C. Subsequently, 0.5 mL of polyethylene glycol (PEG) was introduced into the cationic solution. Finally, a solution comprising 0.01 M of Na_2S (0.1200 g for each sample) in 50 mL of deionized water was gradually added to the prior solution, which was then vigorously stirred for 8 h at 120 °C. The resultant sediment was sterilized using ethanol and distilled water, and then annealed at 150 °C for a duration of 1 day.

2.2. Characterizations

The samples prepared underwent comprehensive analysis, employing a variety of advanced techniques. High-resolution transmission electron microscopy (Philips Tecnai FE 12 model, Dallas, TX, USA) was employed to scrutinize their morphology. Surface analysis

of the fabricated samples was employed with field emission scanning electron microscope (HITACHI S-4200 model, Tokyo, Japan). The chemical composition and stoichiometry were thoroughly examined through X-ray photoelectron spectroscopy (Thermo Scientific K-Alpha, Waltham, MA, USA). Diffuse reflectance spectroscopy (DRS) measurements were carried out, utilizing a cutting-edge UV–vis–NIR double-beam spectrophotometer (Cary 5000, Santa Clara, CA, USA). Raman spectra were acquired by utilizing a sophisticated Raman spectrometer (Nicolet 6700, Temecula, CA, USA) with a 532-nanometer laser source. X-ray diffraction (XRD) patterns were meticulously recorded using a state-of-the-art X-ray diffractometer (PAN analytical, London, UK).

Photocatalytic hydrogen (H_2) production measurements were conducted using a 150 mL quartz reactor at room temperature under controlled conditions. For each experiment, 5 mg of the prepared photocatalyst samples were dispersed in 50 mL of an aqueous solution containing 0.25 mol L^{-1} Na_2SO_3 and Na_2S as sacrificial agents, serving as electron donors to suppress charge carrier recombination. A 300 W Xe lamp (MaX 303 model, Asahi Spectra Co., Ltd. Tokyo, Japan) was employed as a simulated solar light source with an intensity of 50 mW cm^{-2} to ensure efficient light absorption by the photocatalysts. Before irradiation, the reactor was thoroughly evacuated using a vacuum pump and purged with nitrogen gas (N_2) for 20 min to remove residual air and create an inert atmosphere, preventing interference from oxygen during the reaction. The generated hydrogen gas was quantified using an offline gas chromatograph (GC, YL-6500 model, YL Instruments, Anyang, Republic of Korea) equipped with a thermal conductivity detector and a 5A molecular sieve column, ensuring precise and reliable measurements. This setup facilitated a controlled and reproducible evaluation of the photocatalytic performance of the synthesized materials.

3. Results and Discussion

3.1. X-Ray Diffraction Studies

Figure 1 illustrates the XRD patterns of the CdS, CdS:Ce, and CdS:(Ce, Ga) nanoparticles. The patterns obtained acknowledge that these nanoparticles have three major diffraction characters belonging to (111), (220), and (311) planes and can be evidenced to a standard JCPDS file number 80-0019 of bulk cubic CdS [14]. The lack of additional reflection peaks related to Ce and Ga stipulate the high quality of the eventual product. The enormous peaks trivially shift towards a higher angle direction on Ce-doping and (Ce, Ga) co-doping in comparison to that of pristine CdS. The lattice constants of Ce-doped and (Ce, Ga) co-doped CdS samples are slightly smaller than those of pure CdS samples. Lattice parameters can be assessed from the (111) plane of the prepared samples as 0.542 nm for CdS, 0.541 nm for CdS:Ce, and 0.539 nm for CdS:(Ce, Ga) samples, respectively. The reduction in lattice constant suggests the successful incorporation of Ce and Ga into the CdS matrix, where they substitute the Cd (II) sites. This substitution occurs due to the mismatch in ionic radii, with Ce (0.103 nm) and Ga (0.062 nm) ions differing from the Cd (0.097 nm) ions. Moreover, the breadth of the diffraction peaks of the Ce-doped and (Ce, Ga) co-doped samples broadens because of the lower average diameters. Based on the Debey–Scherrer's equation, the estimated average crystallite sizes of the prepared samples are 6.1 nm, 5.7 nm, and 5.2 nm for the CdS, CdS:Ce, and CdS:(Ce, Ga) samples. In general, the inclusion of Ce and (Ce, Ga) ions in the host matrix is known to influence the growth character and is thus responsible for the reduction in particle size after Ce-doping and (Ce, Ga) co-doping. Saravanan et al. [15] reported the hexagonal structure of the nanocrystalline CdS:Ce via a co-precipitation route. Giribabu et al. [16] observed the zinc blende structure of CdS:(Co, Mn) nanoparticles.

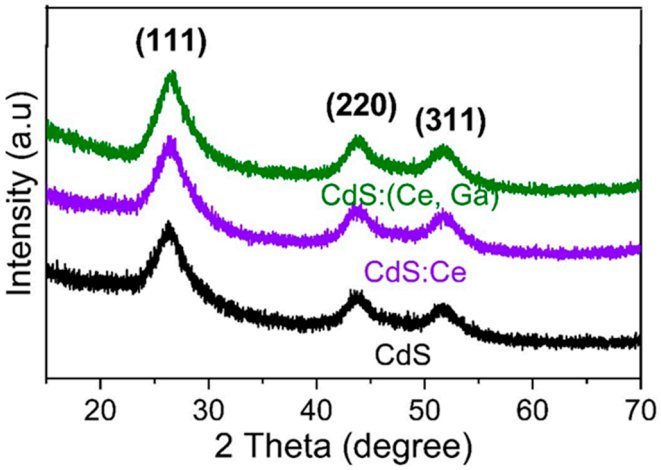

Figure 1. XRD patterns of the CdS, CdS:Ce, and CdS:(Ce, Ga) samples.

3.2. Micro-Raman Studies

Raman spectra of pristine CdS, CdS:Ce, and CdS:(Ce, Ga) nanoparticles at room temperature were collected to provide additional confirmation of their structural characteristics. Figure 2 depicts the Raman spectra of the prepared samples. These spectra display a prominent peak at 303.8 cm^{-1}, alongside a subtle vibration peak at 603.3 cm^{-1}. The prime node at 303.8 cm^{-1} is attributed to the A_1 longitudinal optical mode (1LO). The secondary peak at 603.3 cm^{-1} could be attributed to the longitudinal optical mode (2LO). The appearance of two nodes in these spectra identically stipulates that the prepared materials are a cubic phase that includes a pure CdS system. Foreign nodes related to impurities were not found in the prepared samples, evidencing the good quality of the synthesized materials. Similar kinds of reports have been published by many research groups [14,17].

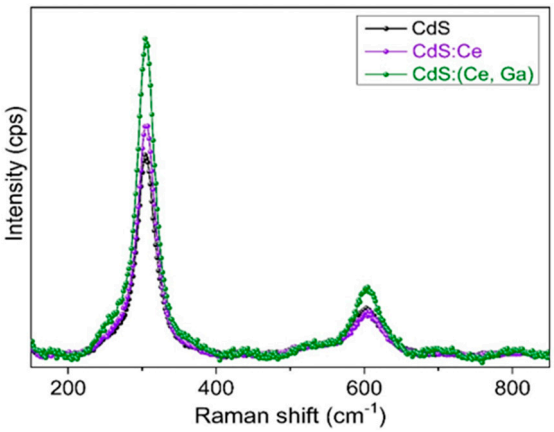

Figure 2. Raman spectra of the CdS, CdS:Ce, and CdS:(Ce, Ga) samples.

3.3. Morphology Studies

Figure 3 represents the FESEM pictures of the (a) CdS, (b) CdS:Ce, and (c) CdS:(Ce, Ga) samples. It is evident that all the synthesized materials are agglomerated. HRTEM was utilized to accurately determine the size of the nanoparticles. Figure 4a–c illustrates the HRTEM images of (a) CdS, (b) CdS:Ce, and (c) CdS:(Ce, Ga) samples. The analysis revealed that the average size of the synthesized nanoparticles was approximately 5 nm. These findings are consistent with the results obtained from X-ray diffraction studies. The micrographs also show that the nanoparticles exhibit slight agglomeration and irregular shapes, which is a common characteristic observed in II-VI semiconductor nanoparticles [18,19].

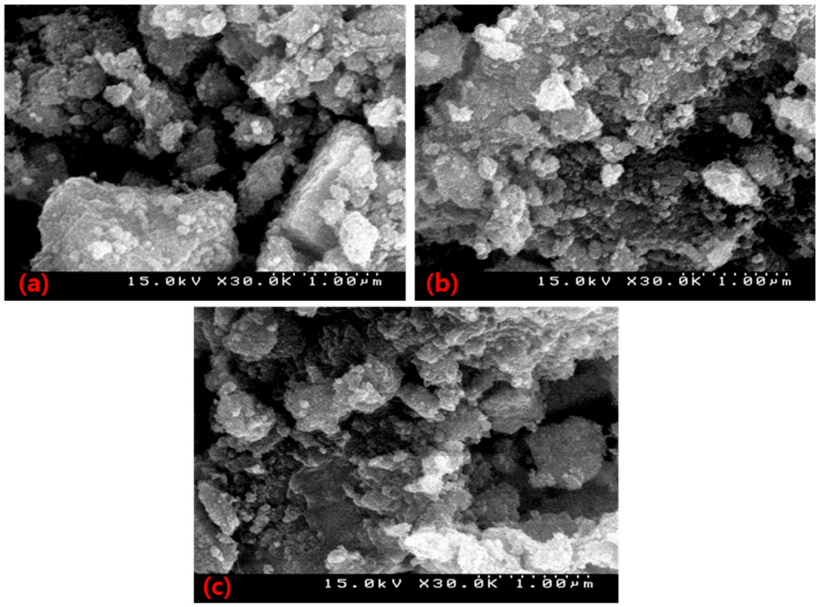

Figure 3. FESEM images of (**a**) CdS, (**b**) CdS:Ce, and (**c**) CdS:(Ce, Ga) samples.

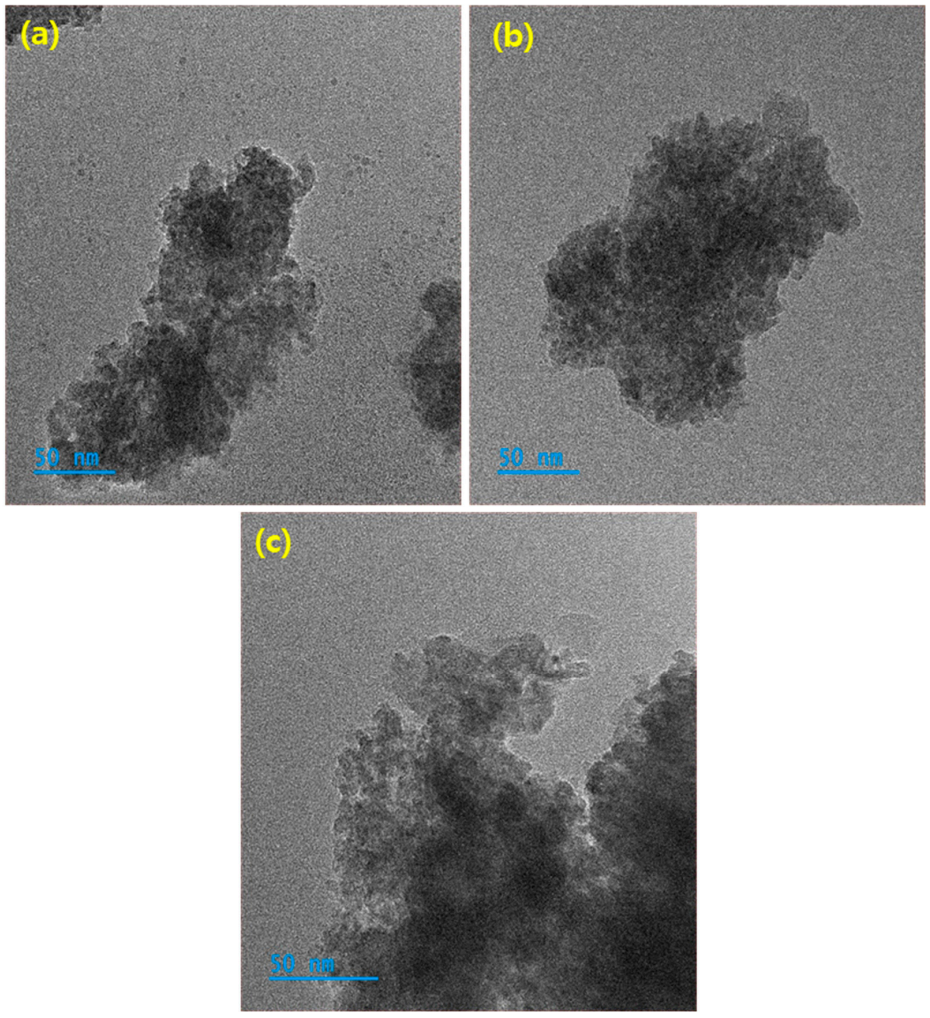

Figure 4. HRTEM images of (**a**) CdS, (**b**) CdS:Ce, and (**c**) CdS:(Ce, Ga) samples.

3.4. Chemical Studies

Figure 5a stipulates the X-ray photoelectron spectroscopy survey scan of the CdS:(Ce, Ga) sample. It distinctly shows the presence of cadmium and sulfur elements in the

pure CdS sample (Figure 5) and of cadmium, sulfur, cerium, and gallium elements in the CdS:(Ce, Ga) sample. In addition, oxygen peaks can be seen. In general, the presence of oxygen peaks is a common observation in the XPS of nanoparticles due to their high surface area, reactivity, and susceptibility to environmental exposure and oxidation. The obtained stoichiometric ratios are very close to the initial targeted values. Figure 5b–e displays the high-resolution scans of cadmium, sulfur, cerium, and gallium elements for the CdS:(Ce, Ga) sample. In Figure 5b, two distinct and prominent peaks are observed at binding energies of 776.34 eV and 887 eV, which correspond to Cd $2P_{3/2}$ and Cd $2P_{1/2}$, respectively, indicating the presence of the divalent chemical state of Cd [16]. Figure 5c displays the high-resolution S 2p spectra, revealing two prominent peaks at binding energies of 160.85 and 162.02 eV. These peaks are associated with the spin–orbit split states, $2p_{3/2}$ and $2p_{1/2}$, of S^{2-} [20]. In Figure 5d, the high-resolution XPS scan of gallium shows two peaks at binding energies of 1118.12 eV and 1144.98 eV, assigned to Ga $2p_{3/2}$ and Ga $2p_{1/2}$, respectively. This confirms the trivalent existence of Ga ions in the CdS [20]. In Figure 5e, the XPS narrow scan of cerium reveals four peaks at 883.88, 889.67, 901.10, and 916.93 eV, corresponding to Ce (III) $3d_{5/2}$, Ce (IV) $3d_{5/2}$, Ce (III) $3d_{3/2}$, and Ce (IV) $3d_{3/2}$, respectively. These observations confirm the existence of both 3+ and 4+ valence states of the cerium ions within the CdS matrix [21]. At the same time, the lack of additional foreign peaks related to the Ce and Ga ions indicate the impurity-free characteristic of the synthesized materials.

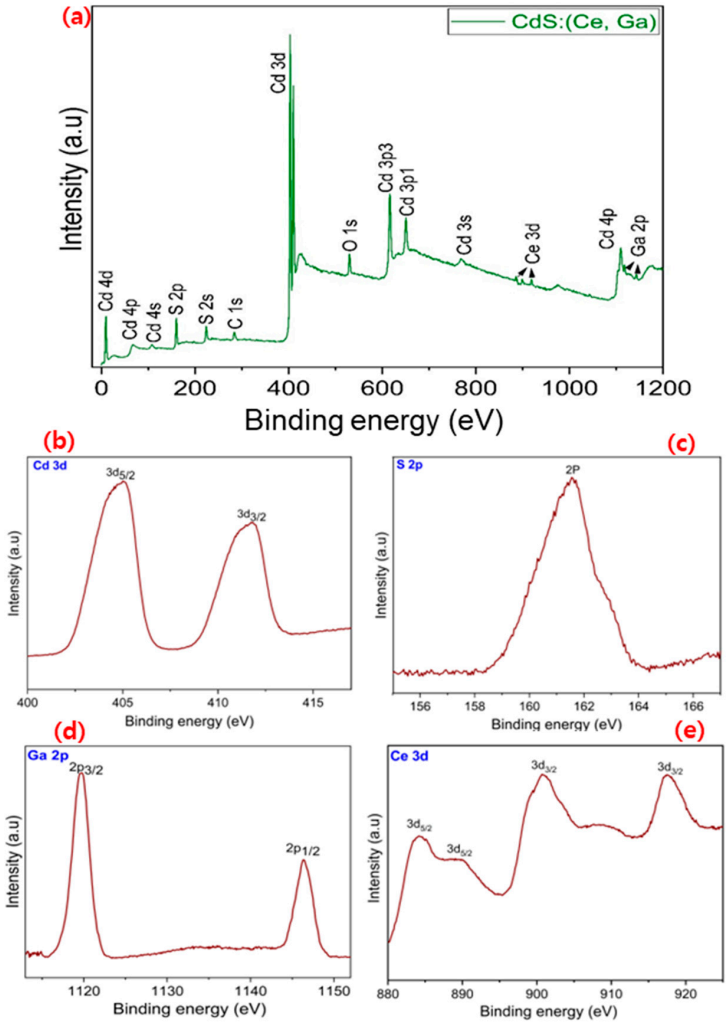

Figure 5. XPS (**a**) survey scan, narrow scans of (**b**) Cd, (**c**) S, (**d**) Ga, and (**e**) Ce of the CdS:(Ce, Ga) sample.

3.5. Optical and Photoluminescence Studies

Tuning and analyzing the energy band gap of semiconductors is vital for optimizing their performance in electronic applications. The band gaps of the CdS, CdS:Ce, and CdS:(Ce, Ga) nanoparticles were determined through DRS, as shown in Figure 6a. The spectra indicate reflectance peaks in the 500–650 nm range for the synthesized nanoparticles. A noticeable redshift in the absorption edge occurred following Ce-doping and (Ce, Ga) co-doping, shifting toward longer wavelengths. This shift highlights the successful incorporation of Ce and Ga ions into the CdS lattice, accompanied by a reduction in the optical band gap, which underscores the impact of doping on the material's electronic properties. Figure 6b illustrates the photoluminescence (PL) spectra of CdS, CdS:Ce, and CdS:(Ce, Ga) samples. The undoped CdS sample exhibits two prominent emission peaks at 530 nm (green) and 691 nm (red). After Ce-doping, these peaks shift slightly toward higher wavelengths, appearing at 538 nm and 695 nm, respectively. A further redshift is observed in the (Ce, Ga) co-doped sample, with peaks at 547 nm and 699 nm. These shifts indicate the successful incorporation of dopants into the CdS lattice. The green emission peak is attributed to the migration of charge carriers from defect states to the valence band, while the red emission likely originates from Cd vacancies created by the substitution of Ce and Ga ions [22,23]. Moreover, the PL intensity gradually decreases upon doping and co-doping, which is attributed to the suppression of charge carrier recombination. This reduction in fluorescence efficiency is a common phenomenon in doped semiconductor systems [23,24]. The lower PL intensity in the (Ce, Ga) co-doped samples suggests a higher availability of free charge carriers, making these materials particularly effective for hydrogen generation and photocatalytic applications. Similarly, our previous study demonstrated a reduction in PL intensity following erbium doping in CdS nanoparticles [23]. Giribabu et al. [22,24] also reported a decline in fluorescence efficiency in CdS:Co nanoparticles after Mn and Al co-doping.

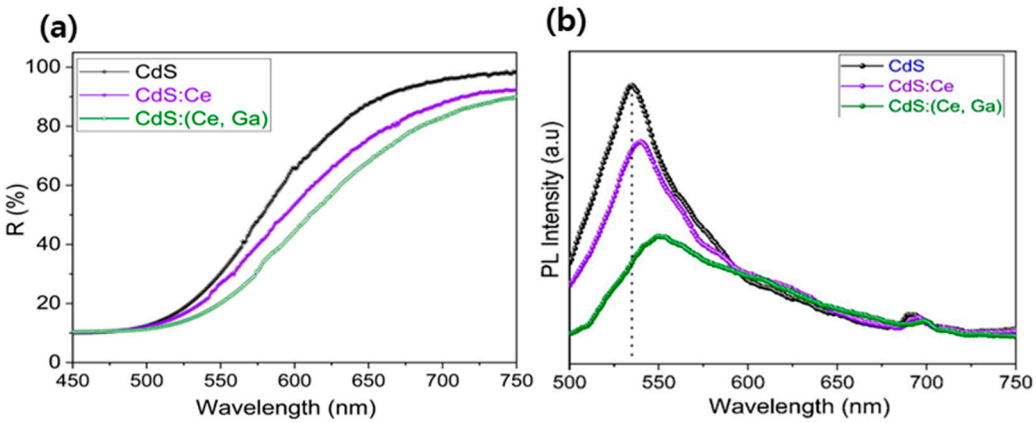

Figure 6. (**a**) DRS spectra and (**b**) PL spectra of CdS, CdS:Ce, and CdS:(Ce, Ga) sample.

3.6. Photocatalytic H_2 Production Studies

It was explored to produce innovative photocatalysts in modest and sustainable conditions for H_2 evolution. The H_2 evolution performances of the CdS, CdS:Ce, and CdS:(Ce, Ga) samples were investigated in water under simulated solar illumination, with lactic acid employed as a scavenger agent in the reaction medium. Figure 7a showcases the H_2 evolution of the CdS, CdS:Ce, and CdS:(Ce, Ga) samples over a 300 min constant time course under artificial solar illumination. The H_2 production rate was around 216 (µmol/gm) for the pure CdS sample, notably reduced due to the rapid recombination of electrons and holes, as well as the photo-corrosion effect [25]. Concurrently, the introduction of Ce-doping and (Ce, Ga) co-doping into the CdS system led to a linear elevation in the rate of

H_2 production. The H_2 yield for the CdS:Ce and CdS:(Ce, Ga) samples was 1389 (µmol/gm) and 3012 (µmol/gm), respectively. The H_2 production rate of the CdS:(Ce, Ga) sample was nearly 13.9 times larger than that of the CdS samples and 2.1 times larger than that of the CdS:Ce sample. The heightened H_2 production efficiency of the CdS:(Ce, Ga) sample could be attributed to several factors. Primarily, the emergence of abundant charge carriers due to the (Ce, Ga) co-doping process plays a crucial role. Additionally, the presence of defective sites and trap locations contributes to this enhancement. Ultimately, the reduction in the recombination rate between charge carriers serves as a fundamental mechanism driving the effective photocatalytic H_2 production observed in the CdS:(Ce, Ga) sample [26,27].

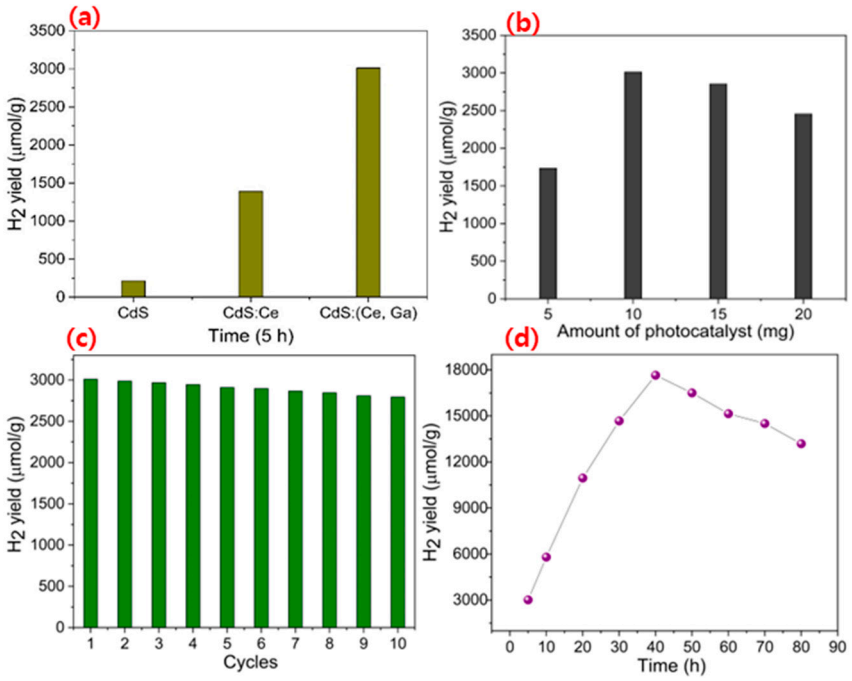

Figure 7. (**a**) H_2 evolution, (**b**) catalyst dosage, (**c**) durability, and (**d**) stability test for the CdS:(Ce, Ga) sample.

In the photocatalytic mechanism, the fabricated catalyst materials play a pivotal role in H_2 evolution. Crucially, determining the optimal dose concentration is essential to avoid catalyst wastage and ensure efficient H_2 production. Therefore, we conducted dose concentration tests to evaluate the H_2 yield potential. The results indicate that a dose of 10 mg of the CdS:(Ce, Ga) sample is most favorable for achieving maximum H_2 efficiency. As presented in Figure 7b, the outcomes reveal a gradual decline in the H_2 evolution rate beyond the optimal point. This decline can be attributed to the aggregation of nanoparticles and the onset of turbulence in the reaction suspension. These factors effectively restrict light penetration into the aqueous media, consequently mitigating the rate of H_2 production. For realistic use, the recyclability, and stability of the CdS:(Ce, Ga) sample in aqueous solution are the most important concerns.

Figure 7c illustrates the H_2 production rate versus the recyclability times of the CdS:(Ce, Ga) sample at regular intervals. It is clear that the rate of H_2 production remains consistent over ten complete cycles, showcasing the remarkable stability and optimal performance of the CdS:(Ce, Ga) sample. These results validate the effectiveness of the designed nanoparticles for achieving consistent and efficient photocatalytic H_2 production. Figure 7d portrays the stability assessment of the CdS:(Ce, Ga) sample over an 80 h period. Notably, the rate of H_2 production gradually increases with reaction time, peaking at 60 h before showing a slight decline. This trend suggests the accumulation of H_2 gas in the reaction chamber over time. In Figure 7, a schematic illustration elucidates the process: lactic acid molecules

serve as sacrificial agents to capture holes; Ce dopant and (Ce, Ga) co-dopant ions generate an abundance of negative charge electrons; meanwhile, CdS, as a wide band gap material, efficiently absorbs visible light. When activated by artificial photons in an aqueous suspension, electrons are emitted from the valence band due to the breaking of covalent bonds between semiconductor atoms. As the electrons transition to the conduction band, leaving holes in the valence band, sacrificial agents like lactic acid capture these holes, transforming them into pyruvic acid. Meanwhile, the electrons remain in the conduction band of the CdS matrix. These free electrons swiftly migrate to the semiconductor surface, where they combine with electrons from Ce dopant and (Ce, Ga) co-dopant ions, forming a substantial electron cloud. This electron abundance greatly facilitates the evolution of H_2. In summary, the CdS:(Ce, Ga) sample stands out as a definitive and efficient material for effective photocatalytic H_2 production. To provide further evidence of the presence of charge carriers in the fabricated nanoparticles, electrochemical impedance spectroscopic measurement was utilized, as depicted in Figure 8a. It is apparent that compared to the CdS, CdS:Ce and, samples, CdS:(Ce, Ga) sample exhibits appreciable semicircle behavior and shows lower resistivity and superior conductivity features. Later, the smaller resistivity of the CdS:(Ce, Ga) samples promotes potential H_2 production because of its superior charge transportation capabilities. In Figure 8b, the photocurrent responses of the CdS, CdS:Ce, and CdS:(Ce, Ga) samples are depicted. Photos stimulate charge carriers, such as electrons and holes, and their transport to the surface of prepared nanoparticles was assessed through transient photocurrent response at equal time intervals. Notably, the CdS:(Ce, Ga) sample demonstrates a significantly larger current density compared to the other materials, attributed to its remarkable capabilities to absorb visible light in electromagnetic radiation. Furthermore, upon switching off the simulated light, the photocurrent intensity experienced a sudden decrease, indicating the transport of charge carriers towards the electrodes. Hence, the thorough analyses above distinctly proposed that the CdS:(Ce, Ga) sample is beneficial for efficient H_2 production via water splitting. In our previous studies, we recognized the maximum H_2 production in a gadolinium-co-doped CdS:Cr system and erbium-doped CdS nanoparticles through a co-precipitation method [16,23]. Recently, Mohanad et al. [28] reported an enriched H_2 production (26.2%) rate in a Tb-doped CdS system. Most recently, Liu et al. [29] achieved a higher H_2 evolution rate in CdS/Au on $BiVO_4$ with a gold-free photocatalyst. Numerous intriguing and significant findings related to photocatalytic hydrogen production have been reported in recent publications [30–33].

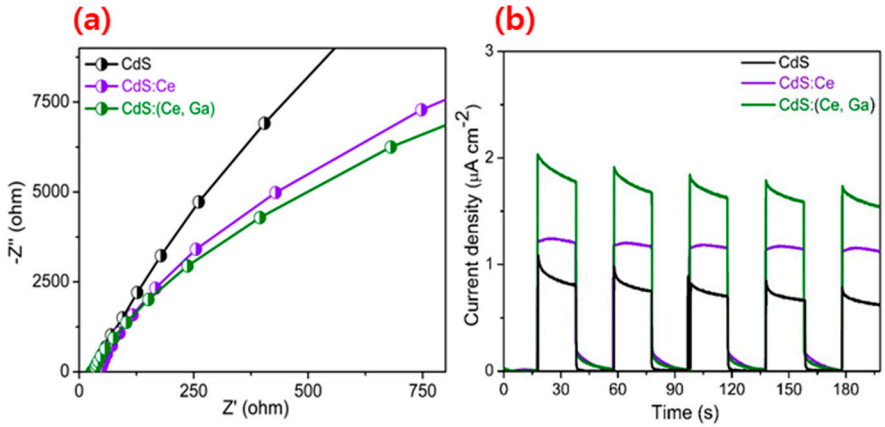

Figure 8. (**a**) EIS and (**b**) photocurrent studies of the CdS, CdS:Ce, and CdS:(Ce, Ga) sample.

4. Conclusions

In summary, we effectually synthesized easy and potent photocatalytic nanoparticles of CdS, CdS:Ce, and CdS:(Ce, Ga) for H_2 evolution. Comprehensive structural measure-

ments indicate that the Ce and (Ce, Ga) ions are substituted into the bare CdS matrix without altering its earliest structure. The CdS:(Ce, Ga) sample displayed an efficient H_2 production capability (3012 μmol $h^{-1}g^{-1}$) in 300 min, which was larger than that of the CdS and CdS:Ce samples. Hence, the CdS:(Ce, Ga) sample is dependable potential semiconductor material for effective photocatalytic H_2 production.

Author Contributions: P.T.P.: Conceptualization, Methodology, Experimental, Investigation, and Writing—original draft. R.D., M.R.K. and S.J.A.: Methodology, and characterization. K.M.R. and S.P.R.M.: Writing—Review, Validation, Editing, and Resources. Y.L.K.: Investigation, Formal Analysis, Editing, Writing—Review, and Supervision. All authors have read and agreed to the published version of the manuscript.

Funding: This work was supported by "Regional Innovation Strategy (RIS)" through the NRF funded by the Ministry of Education (MOE) (2022RIS-005). The authors extend their appreciation to the Research Supporting Project number (RSPD2025R956), King Saud University, Riyadh, Saudi Arabia. This study was partially supported by the National Research Foundation of Korea (NRF) founded by the Ministry of Science (2022R1I1A1A01064248) and (2018R1A6A1A03025761).

Data Availability Statement: Data available on request.

Conflicts of Interest: The authors declare no conflicts of interest.

References

1. Kazemi, A.; Manteghi, F.; Tehrani, Z. Metal Electrocatalysts for Hydrogen Production in Water Splitting. *ACS Omega* **2024**, *9*, 7310–7335. [CrossRef] [PubMed]
2. Xue, X.; Dong, W.; Luan, Q.; Gao, H.; Wang, G. Novel interfacial lateral electron migration pathway formed by constructing metallized CoP_2/CdS interface for excellent photocatalytic hydrogen production. *Appl. Catal. B Environ.* **2023**, *334*, 122860. [CrossRef]
3. Lalitha, K.; Sadanandam, G.; Kumari, V.D.; Subrahmanyam, M.; Sreedhar, B.; Hebalkar, N.Y. Highly stabilized and finely dispersed Cu_2O/TiO_2: A promising visible sensitive photocatalyst for continuous production of hydrogen from glycerol: Water mixtures. *J. Phys. Chem. C* **2010**, *114*, 22181–22189. [CrossRef]
4. Bak, D.; Kim, J.H. Facile fabrication of pseudo-microspherical ZnO/CdS core-shell photocatalysts for solar hydrogen production by water splitting. *Ceram. Int.* **2017**, *43*, 13493–13499. [CrossRef]
5. Dedong, H.; Kai, L.Y.; Yu, D.P. Multicolor photodetector of a single Er^{3+} doped CdS Nanoribbon. *Nanoscale Res. Lett.* **2015**, *285*, 1–10. [CrossRef]
6. Zhai, J.; Wang, L.; Wang, D.; Li, H.; Zhang, Y.; He, D.Q.; Xie, T. Enhancement of gas sensing properties of CdS Nanowire/ZnO nanosphere composite materials at room temperature by visible-light activation. *ACS Appl. Mater. Interfaces* **2011**, *3*, 2253–2258. [CrossRef]
7. Yuan, Y.J.; Chen, D.; Yu, Z.T.; Zou, Z.G. Cadmium sulfide-based nanomaterials for photocatalytic hydrogen production. *J. Mater. Chem. A* **2018**, *6*, 11606–11630. [CrossRef]
8. Su, J.; Zhang, T.; Li, Y.; Chen, Y.; Liu, M. Photocatalytic activities of copper doped cadmium sulfide microspheres prepared by a facile ultrasonic spray-pyrolysis method. *Molecules* **2016**, *21*, 735. [CrossRef]
9. Ma, Y.; Hai, G.; Liu, J.; Bao, J.; Li, Y.; Wang, G. Enhanced visible light photocatalytic hydrogen evolution by intimately contacted Ni_2P decorated Ni-doped CdS nanospheres. *Chem. Eng. J.* **2022**, *441*, 136002. [CrossRef]
10. Cheng, L.; Xiang, Q.; Liao, Y.; Zhang, H. CdS-Based photocatalysts. *Energy Environ. Sci.* **2018**, *11*, 1362–1391. [CrossRef]
11. Chen, X.; Shangguan, W. Hydrogen production from water splitting on CdS-based photocatalysts using solar light. *Front. Energy.* **2013**, *7*, 111–118. [CrossRef]
12. Fan, L.; Han, J.; Wei, K.; Ma, C.; Feng, S.; Zhou, Y.; Dai, X.; Ye, Z.; Wang, Y. Mn-doped CdS/Cu_2O: An S-scheme heterojunction for photocatalytic hydrogen production. *J. Alloys Compd.* **2023**, *960*, 170382. [CrossRef]
13. Chen, T.; Yang, C.; Rajendran, S.; Sawangphruk, M.; Zhang, X.; Qin, J. Utilizing the built-in electric field of p-n heterojunction to spatially separate the photogenerated charges in C, N co-doped Co_3O_4/CdS photocatalysts. *Fuel* **2023**, *331*, 125594–125604. [CrossRef]
14. Poornaprakash, B.; Reddy, B.P.; Prasad, P.R.; Reddy, A.S.; Subramanyam, K.; Reddy, M.S.P.; Tighezza, A.M.; Sangaraju, S.; Park, S.H.; Kwon, M.W.; et al. Synthesis of highly efficient (Cr, Gd) co-doped CdS quantum dots for photocatalytic H_2 evolution beneath artificial solar light irradiation. *Ceram. Int.* **2024**, *50*, 6120–6127. [CrossRef]

15. Saravanan, L.; Pandurangan, A.; Jayavel, R. Synthesis and luminescence enhancement of Cerium doped CdS nanoparticles. *Mater. Lett.* **2012**, *66*, 343–345. [CrossRef]
16. Giribabu, G.; Murali, G.; Reddy, D.A.; Liu, C.; Vijayalakshmi, R.P. Structural, optical and magnetic properties of Co doped CdS nanoparticles. *J. Alloys Compd.* **2013**, *581*, 363–368. [CrossRef]
17. Poornaprakash, B.; Subramanyam, K.; Cheruku, R.; Kim, Y.L.; Reddy, M.S.P.; Reddy, V.R.M. Mn and Al co-doped CdS:Cr nanoparticles for spintronic applications. *Mater. Sci. Semicond. Process.* **2021**, *134*, 106055. [CrossRef]
18. Beketov, I.V.; Safronov, A.P.; Medvedev, A.I.; Alonso, J.; Kurlyandskaya, G.V.; Bhagat, S.M. Iron oxide nanoparticles fabricated by electric explosion of wire: Focus on magnetic nanofluids. *AIP Adv.* **2012**, *2*, 022154. [CrossRef]
19. Poornaprakash, B.; Poojitha, P.T.; Chalapathi, U.; Ramu, S.; Vijayalakshmi, R.P.; Park, S.H. Chemical synthesis, compositional, morphological, structural, optical and magnetic properties of $Zn_{1-x}Dy_xS$ nanoparticles. *Ceram. Int.* **2016**, *42*, 8092–8097. [CrossRef]
20. Poornaprakash, B.; Chalapathi, U.; Vattikuti, S.V.P.; Sekhar, M.C.; Reddy, B.P.; Poojitha, P.T.; Reddy, M.S.P.; Suh, Y.; Park, S.H. Enhanced fluorescence efficiency and photocatalytic activity of ZnS quantum dots through Ga doping. *Ceram. Int.* **2019**, *45*, 2289–2294. [CrossRef]
21. Poornaprakash, B.; Chalapathi, U.; Subramanyam, K.; Vattikuti, S.V.P.; Suh, Y.; Park, S.H. Effects of Ce incorporation on the structural, morphological, optical, magnetic, and photocatalytic characteristics of ZnO nanoparticles. *Mater. Res. Express* **2019**, *6*, 125075. [CrossRef]
22. Giribabu, G.; Murali, G.; Reddy, D.A.; Sambasivam, S.; Vijayalakshmi, R.P. Structural, optical and magnetic properties of cobalt and aluminum codoped CdS nanoparticles. *Mater. Lett.* **2014**, *126*, 119–122. [CrossRef]
23. Poornaprakash, B.; Chalapathi, U.; Kumar, M.; Subramanyam, K.; Vattikuti, S.V.P.; Reddy, M.S.P.; Park, S.H. Enhanced photocatalytic activity and hydrogen evolution of CdS nanoparticles through Er doping. *Ceram. Int.* **2020**, *46*, 21728–21735. [CrossRef]
24. Giribabu, G.; Murali, G.; Vijayalakshmi, R.P. Structural, magnetic and optical properties of cobalt and manganese codoped CdS nanoparticles. *Mater. Lett.* **2014**, *117*, 298–301. [CrossRef]
25. Liu, Y.; Ding, S.; Shi, Y.; Liu, X.; Wu, Z.; Jiang, Q.; Zhou, T.; Liu, N.; Hu, J. Construction of CdS/CoO_x core-shell nanorods for efficient photocatalytic H2 evolution. *Appl. Catal. B Environ.* **2018**, *234*, 109–116. [CrossRef]
26. Han, B.; Liu, S.; Zhang, N.; Xu, Y.Z.; Tang, Z.R. One-dimensional CdS@ MoS_2 core-shell nanowires for boosted photocatalytic hydrogen evolution under visible light. *Appl. Catal. B Environ.* **2017**, *202*, 298–304. [CrossRef]
27. Yin, X.L.; Li, L.L.; Jiang, W.J.; Zhang, Y.; Zhang, X.; Wan, L.J.; Hu, J.S. MoS_2/CdS nanosheets-on-nanorod heterostructure for highly efficient photocatalytic H_2 generation under visible light irradiation. ACS Appl. *Mater. Interfaces* **2016**, *8*, 15258–15266. [CrossRef]
28. Murish, M.A.; Autade, V.; Barimah, E.K.; Panmand, R.; Kale, B.; Jh, A. Engineering of Solar Energy Harvesting Tb^{3+}-Ion-Doped CdS Quantum Dot Glasses for Photodissociation of Hydrogen Sulfide. *ACS Appl. Energy Mater.* **2023**, *6*, 8875–8888.
29. Liu, M.H.; Takahashi, Y. Boosting photocatalytic hydrogen production of $CdS/BiVO_4$ nanoplates by transferring in-plane plasmon resonant energy of gold nanoparticles. *Catal. Sci. Technol.* **2014**, *14*, 1756–1759. [CrossRef]
30. Meena, B.; Subramanyam, P.; Suryakala, D.; Biju, V.; Subramanyam, C. Efficient solar water splitting using a CdS quantum dot decorated TiO_2/Ag_2Se photoanode. *Int. J. Hydrogen Energy* **2001**, *46*, 34079–34088. [CrossRef]
31. Sun, B.; Vorontsov, A.V.; Smirniotis, P.G. Role of Platinum Deposited on TiO_2 in Phenol Photocatalytic Oxidation. *Langmuir* **2003**, *19*, 3151–3156. [CrossRef]
32. Sun, B.; Reddy, E.P.; Smirniotis, P.G. Visible Light Cr(VI) Reduction and Organic Chemical Oxidation by TiO_2 Photocatalysis. *Environ. Sci. Technol.* **2005**, *39*, 6251–6259. [CrossRef] [PubMed]
33. Reddy, E.P.; Sun, B.; Smirniotis, P.G. Transition Metal Modified TiO_2-Loaded MCM-41 Catalysts for Visible- and UV-Light Driven Photodegradation of Aqueous Organic Pollutants. *J. Phys. Chem. B* **2004**, *108*, 17198–17205. [CrossRef]

Disclaimer/Publisher's Note: The statements, opinions and data contained in all publications are solely those of the individual author(s) and contributor(s) and not of MDPI and/or the editor(s). MDPI and/or the editor(s) disclaim responsibility for any injury to people or property resulting from any ideas, methods, instructions or products referred to in the content.